Deng, Z., Bender, M., Zus, F., Ge, M., Dick, G., Ramatschi, M., Wickert, J., Löhnert, U., Schön, S.(2011): Validation of tropospheric slant path delays derived from single and dual frequency GPS receivers. - Radio Science, 46, RS6007

DOI: 10.1029/2011RS004687

Validation of tropospheric slant path delays derived from single and dual frequency GPS receivers

Zhiguo Deng,[1] Michael Bender,[1] Florian Zus,[1] Maorong Ge,[1] Galina Dick,[1] Markus Ramatschi,[1] Jens Wickert,[1] Ulrich Löhnert,[2] and Steffen Schön[3]

Received 25 February 2011; revised 22 August 2011; accepted 21 September 2011; published 2 December 2011.

[1] In order to increase the spatial resolution of tropospheric delays derived from GPS observations, existing GPS networks assembled from dual frequency (DF) receivers must be densified. For economic reasons, low-cost single-frequency (SF) receivers are considered for the densification. The Satellite-specific Epoch-differenced Ionospheric Delay model (SEID) was developed at the German Research Centre for Geosciences (GFZ) to derive the ionospheric corrections for SF GPS receivers. Those corrections allow synthesizing a L2 observable for SF receivers, and existing GPS processing packages can analyze the resulting observables (L1 and synthesized L2) using the same methodology as with DF receivers. The SEID model has already been successfully applied to tropospheric Zenith Total Delay (ZTD) and station coordinates estimation. To assess the possibility of densifying an existing GPS network with low-cost SF GPS receivers, observations from 258 German DF GPS stations are treated as observations from SF GPS stations (only L_1 GPS observations are used). While in a previous study ZTD products were validated, in this study Slant Total Delay (STD) and Slant Water Vapor (SWV) products, derived from SF data and the SEID model, are validated using tropospheric products derived from DF data, a Water Vapor Radiometer (WVR) and a numerical weather model.

Citation: Deng, Z., M. Bender, F. Zus, M. Ge, G. Dick, M. Ramatschi, J. Wickert, U. Löhnert, and S. Schön (2011), Validation of tropospheric slant path delays derived from single and dual frequency GPS receivers, *Radio Sci.*, *46*, RS6007, doi:10.1029/2011RS004687.

1. Introduction

[2] The potential of GPS derived tropospheric products for meteorological application has been demonstrated by several scientific studies [*Gutman et al.*, 2004; *Poli et al.*, 2007; *Shoji*, 2009]. In fact, several European weather services improve operational weather forecasts by assimilating near real-time ZTDs provided by different GNSS analysis centers (http://egvap.dmi.dk). As a partner of the European Meteorological Services Network (EUMETNET) GNSS water Vapour Programme (E-GVAP) the German Research Centre for Geosciences (GFZ) in Potsdam provides tropospheric products in near real-time and post-processing mode. In addition to Zenith Total Delay (ZTD) data, Slant Total Delay (STD) data of about 320 European GPS stations are available from the GFZ.

[3] For many meteorological applications, e.g., the reconstruction of the spatiotemporal distribution of tropospheric water vapor, GPS derived tropospheric products with high temporal and spatial resolution are required. Currently, ZTDs are available every 15 minutes and STDs are available every 2.5 min at the GFZ [*Bender et al.*, 2010]. Since the distribution of water vapor is highly variable both in time and space, the ZTD interpolation utilizing existing regional GPS networks is not sufficient for numerical weather prediction especially in summer [*Brockmann and Troller*, 2002]. Therefore the GPS network should be densified, ideally aspiring inter-station distance below 20 km [*Braun et al.*, 1999; *Bender et al.*, 2010].

[4] Due to economic reasons, the densification can be realized with inexpensive GPS single-frequency (SF) receivers. However, a proper modeling of the ionospheric delay is required. Most of the ionospheric delay models based on GPS observations are developed for large regions and cannot capture small scale and rapid ionospheric disturbances. Thus, they are not accurate enough for removing ionospheric delays in SF data. Alternative approaches have been developed by *Rocken et al.* [2000], *Janssen and Rizos* [2005], and *Wanninger* [1995], where additional corrections are generated based on the double differenced observation residuals from the surrounding grid of GPS sites. Although they are efficient even for real-time precise positioning, the application of special analysis software, which development required years, is needed. Since most of the operational GPS processing systems are quite different (software packages like BERNESE, EPOS, GAMIT, or GIPSY) [*Haase et al.*, 2003], it would be expensive and time-consuming to implement

[1] GPS/Galileo Earth Observation, Helmholtz Centre Potsdam, German Research Centre for Geosciences, Potsdam, Germany.
[2] Institute for Geophysics and Meteorology, University of Cologne, Cologne, Germany.
[3] Institut für Erdmessung, Leibniz Universität Hannover, Hannover, Germany.

0048-6604/11/2011RS004687

these approaches into all the existing data processing systems. The Satellite specific Epoch-differenced Ionospheric Delay model (SEID) has been developed at the GFZ for estimating ionospheric corrections of SF receivers embedded in networks of DF receivers [*Deng et al.*, 2009]. With the ionospheric corrections derived using SEID, the SF data can be processed in the same way as the DF data using any existing software package and processing procedure without any change.

[5] In this work STDs derived from SF data and the SEID model were validated using STDs derived from DF data and numerical weather model fields. At a single station, the Slant Water Vapor (SWV) derived from the SF and DF data was validated using observations from a collocated Water Vapor Radiometer (WVR).

2. Tropospheric Slant Total Delay

[6] The STD is proportional to the difference between the travel time of a signal from a satellite to a ground-based receiver in the atmosphere and in vacuum [*Hofmann-Wellenhof et al.*, 2001], which is known as:

$$\mathrm{STD} = \int_S n ds - \int_{S_0} ds. \tag{1}$$

Here, n is the atmospheric refraction index, S is the signal path through the atmosphere, and S_0 is the geometric path. With the refractivity $N = (n - 1) \cdot 10^6$ the slant total delay can be written as:

$$\mathrm{STD} = 10^{-6} \int_S N ds + \int_S ds - \int_{S_0} ds. \tag{2}$$

N is related to the atmospheric quantities by

$$N = N_{dry} + N_{wet} = k_1 \frac{p_d}{T} + k_2 \frac{e}{T} + k_3 \frac{e}{T^2}. \tag{3}$$

where N_{dry} and N_{wet} are the dry and wet refractivity; p_d is the partial pressure of dry air in hPa, e is the partial pressure of water vapor in hPa and T is the temperature in K. The empirically determined constants k_1 = 77.6 K/hPa, k_2 = 70.4 K/hPa and $k_3 = 3.73 \cdot 10^5$ K^2/hPa can be found in [*Bevis et al.*, 1994]. In terms of N_{dry} and N_{wet} the slant path delay can be written as:

$$\mathrm{STD} = 10^{-6} \int_S N_{dry} ds + 10^{-6} \int_S N_{wet} ds + \left[\int_S ds - \int_{S_0} ds \right]. \tag{4}$$

The first two terms on the right hand side are referred to as Slant Dry Delay (SDD) and Slant Wet Delay (SWD). For ground-based GPS receiver the geometric delay due to signal path curvature, i.e. $\int_S ds - \int_{S_0} ds$, is very small and can usually be neglected [*Sokolovskiy et al.*, 2001]. Equation (4) can be expressed as:

$$\mathrm{STD} = \mathrm{SDD} + \mathrm{SWD}. \tag{5}$$

The SWD is highly variable in space and time and can contribute up to 10% of the STD [*Solheim et al.*, 1999]. To separate the SWD from the STD, the SDD is computed from the surface pressure using the Saastamoinen model [*Saastamoinen*, 1973]. The SWD is correlated with the Slant Water Vapor (SWV) and can be obtained with the method suggested by [*Bevis et al.*, 1994]:

$$\mathrm{SWV} = \Pi(T_m)\mathrm{SWD}, \tag{6}$$

The SWV is the integrated amount of water vapor along the path between a transmitting GPS satellite and a receiving antenna. The dimensionless quantity $\Pi(T_m)$ depends on the mean weighted temperature of the atmosphere and can be calculated from surface meteorological measurements. If no meteorological sensor is available at the GPS site the surface pressure can be interpolated from the surface meteorological data from synoptic networks with an accuracy of 0.3 hPa [*Gendt et al.*, 2004].

[7] At GFZ the GPS data are analyzed using the Earth Parameter and Orbit determination System (EPOS) software [*Gendt et al.*, 1999], which is based on least squares adjustment of undifferenced GPS phase measurements. To derive ZTD the Precise Point Positioning (PPP) [*Zumberge et al.*, 1997] mode is applied where precise satellite orbits and clocks as well as Earth Rotation Parameters (ERP) are fixed to known values. The station coordinates are tightly constrained and the ZTDs are modeled as a random-walk process [*Tralli and Lichten*, 1990] with a power density of 15 mm/$\sqrt{\text{hour}}$ and estimated every 15 min as piecewise constants with Global Mapping Function (GMF) [*Boehm et al.*, 2006]. The gradients [*Davis et al.*, 1993; *Bar-Sever et al.*, 1998] are estimated once per hour and the absolute antenna Phase Centre Variations (PCV) model is applied [*Schmid et al.*, 2005].

[8] For a short period of time (from several minutes to hours) the STDs of one station can be modeled by the Zenith Hydrostatic Delay (ZHD), the Zenith Wet Delay (ZWD) and the gradients. The ZHD can be computed rather accurately using the Saastamoinen model and meteorological data, the ZWD and gradient parameters are estimated in the GPS data processing. With the ZHD and the estimated tropospheric parameters the STD can be approximated as:

$$\begin{aligned}\mathrm{STD} = \mathrm{ZHD} \cdot M_h + M_w \cdot [\mathrm{ZWD} + \cot(\varepsilon) \cdot (G_N \cdot \cos(\varphi) \\ + G_E \cdot \sin(\varphi))] + R,\end{aligned} \tag{7}$$

where R is residual; ε and φ are the elevation and azimuth of the GPS observation; M_h and M_w are the hydrostatic and the wet coefficients of mapping function; G_N and G_E are the gradients in north and east direction. The anisotropic part of the tropospheric state is described by the gradients G_N, G_E and the residuals.

3. The SEID Model

[9] Usually, the ionosphere which stretches from a height of about 100 km to 1000 km is represented by a thin shell with an altitude, for example, of 350 km above Earth's surface, i.e., forming a single layer model [*Schaer*, 1999; *Rocken et al.*, 2000; *Brunini and Azpilicueta*, 2010]. In the single layer

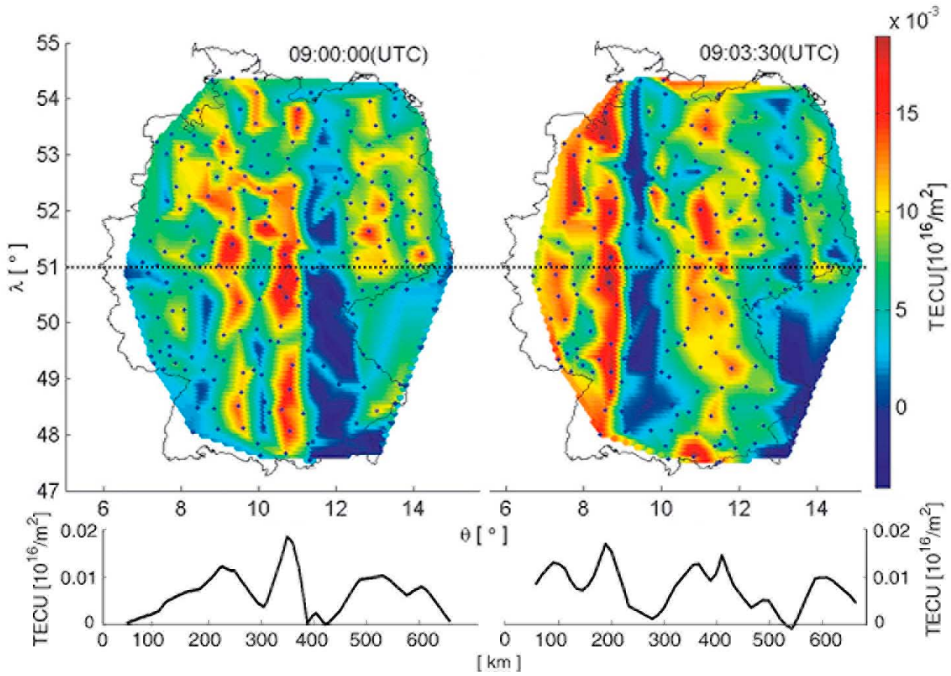

Figure 1. The *dSTEC* distributions for GPS satellite PRN 9 on a single layer for (top left) 09:00:00 UTC and (top right) 09:03:30 UTC at DOY 270 (September 27) in year 2009; PRN 9 had an elevation of about 85°. The dark blue dots are the intercept pierce points of the GPS stations on the 350 km layer above Earth's surface. (bottom) Two *dSTEC* profiles are generated at $\lambda = 51°$ according to the dashed line in Figure 1 (top).

model, the spatial distribution of the ionospheric delay is expressed by the positions of the Intercept Pierce Points (IPP) of the raypaths and the 350 km layer.

[10] The simplified observation equations of the GPS carrier phases L can be expressed as:

$$L_i = \rho - \frac{40.28}{f_i^2} \cdot STEC(\lambda, \theta) + N_i \lambda_i. \tag{8}$$

where ρ is the non-dispersive delay including the geometric delay, the tropospheric delay, and the clock biases; $\frac{40.28}{f_i^2} \cdot STEC(\lambda, \theta)$ denotes the ionospheric delay with the frequency f_i, λ_i is the wavelength, N_i denotes the phase ambiguity, and i is the frequency index. Here STEC is the Slant Total Electron Content, i.e. the line integral of the electron density along a GPS signal path; λ and θ are the latitude and longitude of the IPPs on the layer.

[11] Using L_1 and L_2 the ionospheric observation L_4 (in distance units) is defined as [*Schaer*, 1999]

$$L_4 = L_1 - L_2 = N_1\lambda_1 - N_2\lambda_2 - 40.28\left(\frac{1}{f_1^2} - \frac{1}{f_2^2}\right) \cdot STEC(\lambda, \theta). \tag{9}$$

To reduce the station specific effects, the phase center corrections are applied in advance. Since the ambiguity parameters from the DF stations are unknown and also differ from station to station, the ionospheric corrections for SF stations cannot be directly derived from the L_4 observations of nearby DF stations. To avoid the necessity to estimate the ambiguities of the reference stations the epoch-differences of the ionospheric observations L_4 are used:

$$dL_4(j+1) = L_4(j+1) - L_4(j) = 40.28\left(\frac{1}{f_1^2} - \frac{1}{f_2^2}\right) \cdot dSTEC(\lambda, \theta). \tag{10}$$

The ambiguity is eliminated in $dL_4(j+1)$ between two continuously tracked epochs j and $j+1$. *dSTEC* distributions derived from all DF stations and for GPS satellite PRN9 are given in Figure 1. Two consecutive maps of the *dSTEC* over Germany are shown for 09:00:00 UTC (11:00:00 am, local time, Figure 1, top left) and 09:03:30 UTC (11:03:30 am, local time, Figure 1, top right) at September 27th, 2009 (DOY 270). The elevation of satellite PRN9 was about 85°. In addition two profiles of the *dSTEC* distributions are generated at $\lambda = 51°$. A Medium-Scale Traveling Ionospheric Disturbance (MSTID) wave [*Wanninger*, 1995; *Jakowski et al.*, 2009] moving from east to west across Germany can be observed. Its wavelength is about 300–400 km, with a period of ~7 min.

[12] In a small scale GPS network the *dSTEC* can be fitted to a linear function of the IPP positions of the DF stations. For each GPS satellite and for each pair of epochs j to $j+1$ dL_4 can be approximated by the following observation equation:

$$dL_4(j+1) = a_0 + a_1\lambda + a_2\theta, \tag{11}$$

where a_0, a_1 and a_2 are the model parameters, which describe the change of the ionospheric delay from epoch j to epoch $j+1$ on the shell. The coefficients $a_{0\ldots2}$ can be estimated from the $dL_4(j+1)$ observations of several DF stations by means of a least squares adjustment.

[13] With the estimated model parameters the epoch-differenced ionospheric correction $d\tilde{L}_4(j+1)$ of each SF station can be calculated according to its IPP position. When the ionospheric correction of the SF station at epoch j_n can be continuously tracked from epoch j_0, $\tilde{L}_4$ is the sum of the epoch-differenced corrections between epoch j_0 and j_n:

$$\tilde{L}_4(j_n) = \sum_{j_0}^{j_n} d\tilde{L}_4 + L_4(j_0). \tag{12}$$

As the ionospheric delay L_4 at epoch j_0 is unknown, $\tilde{L}_4(j_n)$ has an unknown constant contribution $L_4(j_0)$, which can be absorbed by the ambiguity.

[14] For each SF receiver the L_2 signal is computed from L_1 and $\tilde{L}_4$:

$$\tilde{L}_2 = L_1 - \tilde{L}_4. \tag{13}$$

The combination L_1 and $\tilde{L}_2$ provides the same information as a DF observation and can be processed exactly in the same way. Thus, no modifications to the processing software are required. It must be pointed out that the ionosphere delay at the first tracked epoch is an arbitrary real value and differs not only for different satellite-station pairs but also for different continuously tracked data pieces of the same pair, and thus can never be cancelled by forming differenced observations between stations and satellites. Therefore, the new ambiguity cannot be fixed to an integer. However, ambiguity-fixing does not improve the ZTD estimates if the data window used in one batch is of appropriate length [*Dousa*, 2001].

4. Validation

4.1. GPS Observations

[15] The data of about 300 German GPS stations were operationally processed by the GFZ in 2007 and a subset of these data was used for this validation study. Most stations belong to the SAtellite POsitioning Service of the German State Survey (SAPOS) but data of other providers such as IAG Reference Frame Sub Commission for Europe (EUREF), German Federal Agency for Cartography and Geodesy (BKG) or GFZ were also available. All stations are equipped with geodetic DF receivers. EPOS (see section 2) was used to analyze the data. The average inter-station distance was about 40 km. Data from 11 days in 2007 were analyzed: August 8–18 (DOY: 220–230).

[16] As a SF GPS network has so far not been established in Germany a simulation study was conducted in order to estimate the potential of a large SF network embedded in the existing DF network. Therefore, the data of the GPS stations were processed in two different ways: At first, the L_1 and L_2 observations from DF stations were used to derive tropospheric products, which were subsequently used as a reference. Second, only the L_1 observations from DF stations were used, the L_2 observations were generated using ionospheric corrections from surrounding DF stations. In this way each station was regarded as a hypothetical SF station embedded in the currently existing DF network. The application of equation (11) requires a minimum of three DF reference stations to estimate the three parameters $a_{0\ldots2}$. More reference stations will improve the reliability and avoid problems caused by missing data. In this study a minimum of 6 and a maximum of 10 reference stations within a radius of 100 km around the hypothetical SF station were used to model the epoch-differenced ionospheric delay.

[17] Both the converted and observed data sets were processed with EPOS in post-processing mode with a sampling interval of 150 s and a cut-off elevation of 7° [*Gendt et al.*, 2004]. The SF data from 258 stations out of the 279 available stations could be processed successfully using the SEID method and EPOS. The $\tilde{L}_2$ signal of the 21 remaining stations could not be determined in this way as the L_2 observations of the surrounding DF stations showed too many gaps. Finally, two sets of tropospheric products were available: STDs (ZTDs) retrieved from DF data and STDs (ZTDs) retrieved from simulated SF data. These tropospheric products were compared with each other and with independent data from a numerical weather model and a water vapor radiometer.

4.2. Comparison of Tropospheric Products From SF and DF Receivers

[18] ZTD observations are the most widely used tropospheric products provided by GPS data processing. The ZTD is in the order of 2.5 m at sea level and shows variations up to 10% mainly caused by the atmospheric humidity. [*Gendt et al.*, 2004] and [*Haase et al.*, 2003] showed that ZTDs derived from DF data have an accuracy of 6–13 mm, when compared to weather model and radiosonde observations.

[19] The ZTD derived from SF data (ZTD_{SF}) were compared to the ZTDs derived from DF data by investigating the difference

$$\delta ZTD = \mathrm{ZTD}_{SF} - \mathrm{ZTD}_{DF}. \tag{14}$$

About 240,000 ZTDs from SF and DF receivers were compared.

[20] The bias is as small as 0.1 mm and the standard deviation is 2.9 mm. In essence the deviation between SF and DF retrieved ZTDs is significantly smaller than the accuracy of DF ZTDs (<6–13 mm). The δZTD histogram (Figure 2, right) shows a rather narrow distribution with very few differences above 5 mm. This is consistent with earlier results presented by [*Deng et al.*, 2009]. The larger differences are mainly caused by some stations with a large RMS above 5 mm (Figure 2, left). Most of them are located at the outer boundaries of the network and it can be assumed that the quality of the ionosphere correction with the SEID method was affected by the unbalanced distribution of the nearby DF stations. The station RMS map also shows that the RMS is rather small in regions of high station density, e. g., in the south-western part, and larger in less dense regions, e. g., the north-western part. Only 8 stations in northwest Germany show an RMS above 6.5 mm. During the selected data period some reference stations in northwest Germany had an unusual large number of small data gaps, which caused additional ambiguities in the converted $\tilde{L}_2$ signal of the 8 stations and corrupted the tropospheric products.

[21] Large numbers of STDs provide spatially resolved information about the atmospheric state and have a consid-

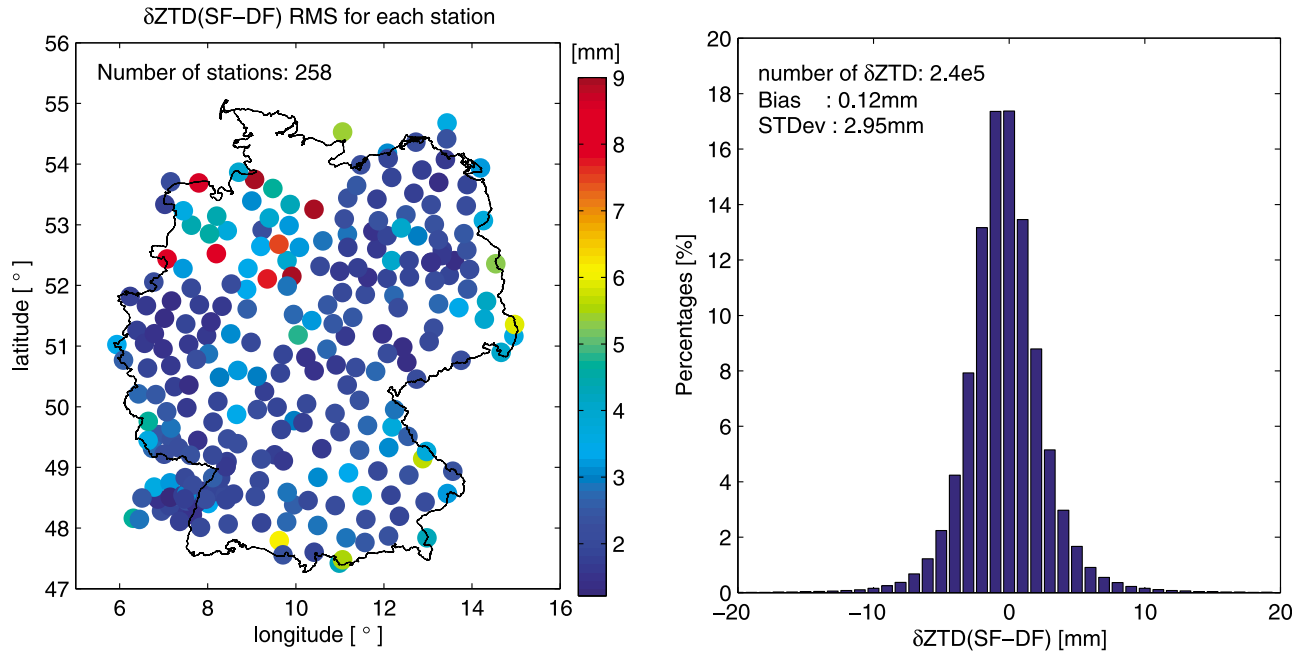

Figure 2. (left) RMS of the ZTD differences between SF and DF stations as computed for each station and frequency histogram of (right) the ZTD differences.

erable potential in future applications e.g., GPS tomography and data assimilation. In zenith direction the STD is ~2.5 m, for lower elevations the STD increases up to ~25 m at $\varepsilon = 5°$. Therefore, absolute differences can only be compared if the elevation is identical and in addition to the absolute STD difference

$$\delta\mathrm{STD} = \mathrm{STD}_{SF} - \mathrm{STD}_{DF}, \tag{15}$$

the fractional STD difference is defined:

$$\delta\mathrm{STD}_{rel} = \frac{\delta\mathrm{STD}}{\mathrm{STD}_{DF}}. \tag{16}$$

[22] About 10 million STDs from SF and DF receivers were compared. Figure 3 (left) shows the bias and the standard deviation between SF and DF STDs versus the elevation angle. For all elevation angles the bias is significantly smaller

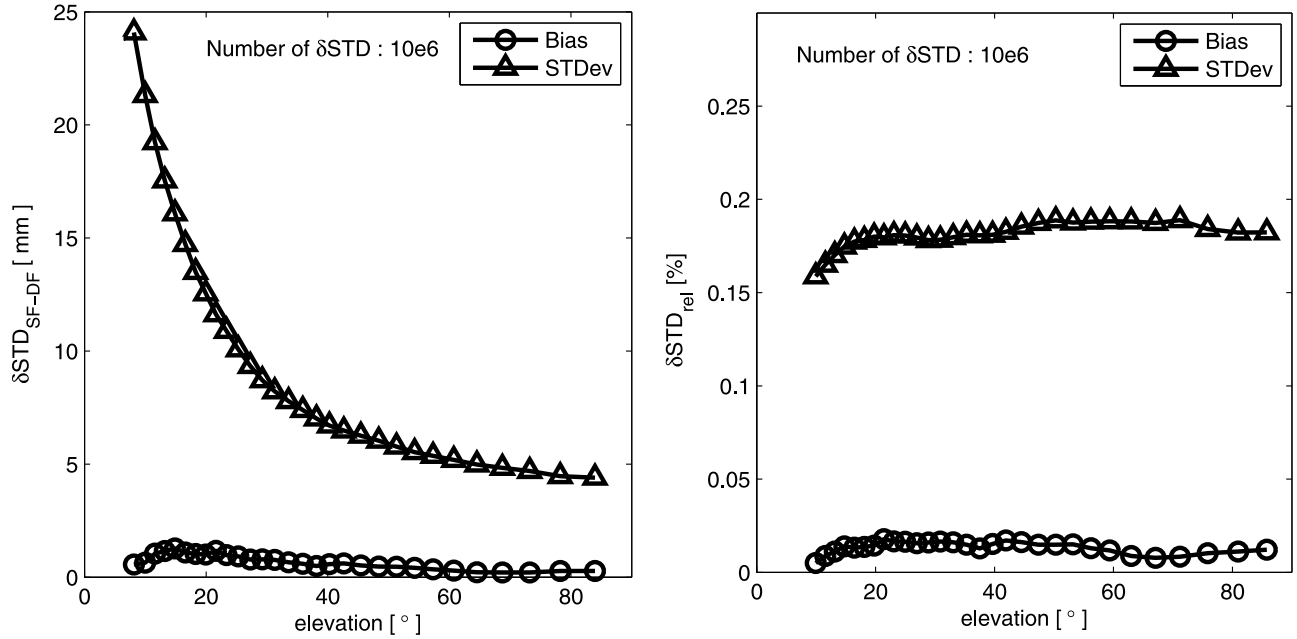

Figure 3. (left) The bias and the standard deviation between SF and DF STDs versus the elevation angle. (right) The fractional bias and standard deviation between SF and DF STDs versus the elevation angle.

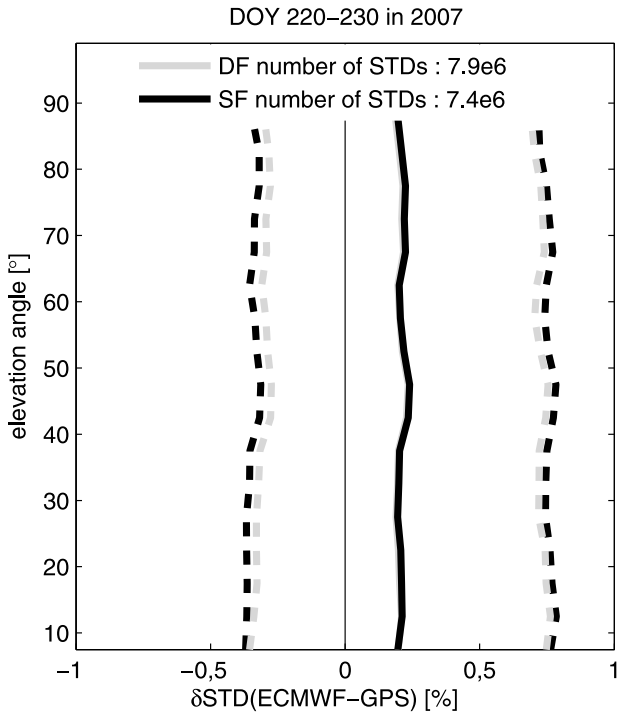

Figure 4. The fractional bias and the standard deviation between GPS retrieved STDs (using SF and DF data) and STDs derived from the ECMWF analysis. The gray (black) lines correspond to the DF (SF) comparison. The solid line indicates the bias, which appear identically for both the SF and DF data. The dashed lines indicate the bias ± standard deviation.

than the standard deviation, i.e. differences between DF and SF STDs are random and not systematic. Close to the zenith the bias and the standard deviations are 0.3 mm and 4.5 mm respectively. The bias and the standard deviation are increasing with decreasing elevation angles and reach 0.6 mm and 24 mm respectively at an elevation angle of 7°. For most applications the STD deviation per unit length or the fractional deviation is much more important. Figure 3 (right) shows the fractional bias and standard deviation between SF and DF STDs versus the elevation angle. The fractional standard deviation is almost constant for all elevation angles and equals ~0.18%, i.e. the relative accuracy of SF STDs, when compared to DF STDs, is not degrading with decreasing elevation angles. Note that the standard deviation between SF and DF ZTDs (σ = 2.9 mm or ~0.13%) is somewhat smaller than the standard deviation between SF and DF STDs close to the zenith. A possible explanation is larger noise in STDs compared to ZTDs.

[23] Comparing DF data processed like hypothetical SF data with real DF observations shows mainly the impact of an imperfect ionosphere modeling on the processed tropospheric products. Real SF data will show some more deficiencies like increased receiver noise, inferior antenna quality, increased multipath effects, etc. The errors estimated here can therefore only be a lower bound for the errors to be expected from real SF observations. However, observations with real SF receivers showed very promising results with errors comparable to the errors found in this simulation study [*Deng et al.*, 2009]. In a future network densification scenario the SF receivers will be placed between the DF stations leading to considerably smaller distances to nearby DF receivers and better ionosphere corrections. No receivers will be installed near the network boundaries or at other unfavorable positions.

4.3. Validation With the ECMWF Model Using Ray-Tracing

4.3.1. Ray-Tracing

[24] In order to compare observed STDs with their model equivalents, ray-tracing through the European Centre for Medium-Range Weather Forecasts (ECMWF) analyses (0.5° × 0.5° horizontal resolution; 91 vertical levels) was performed [*Zus*, 2010]. The ray-trajectory in the ECMWF refractivity field is determined through Fermat's principle: the path taken by a ray between two points, i.e. the ground based receiver and the GPS satellite, minimizes the signal travelling time. From calculus of variations a system of ordinary differential equations is derived and solved by a fully implicit finite difference scheme. Once the ray-trajectory is determined, the STD can be computed according to equation (1). For better efficiency the ray-tracing is restricted to the plane defined by the ground based receiver, the GPS satellite and the center of the Earth. The Earth is assumed to be a perfect sphere with a mean radius being equal to the local curvature radius of the reference ellipsoid at the center point of the ECMWF model domain.

[25] Regarding the expected accuracy of ray-traced STDs it had to be distinguished between uncertainties of STDs due to simplifying assumptions in the ray-tracing algorithm and uncertainties of STDs due to the meteorological variables themselves.

[26] To estimate uncertainties due to simplifying assumptions different interpolation routines were tested, different radii of the Earth were defined and out of plane components were considered in the ray-tracing. In essence, the uncertainty of ray-traced STDs due to simplifying assumptions was estimated to be ~1 mm in the zenith and ~1 cm at an elevation angle of 5°.

[27] The ECMWF meteorological variables themselves (pressure, temperature and humidity), the refractivity field and subsequently the STDs are uncertain. [*Järvinen et al.*, 2007] made an attempt to quantify the uncertainty of STDs due to uncertainty of (typical) numerical weather model refractivity fields. They estimated the uncertainty of STDs to be ~8 mm in the zenith and ~8.4 cm at an elevation angle of 5°.

4.3.2. Intercomparison

[28] The ECMWF analyses are available for 0:00, 6:00, 12:00 and 18:00 UTC. For the 11 days regarded here STDs retrieved from GPS data were compared with their model equivalents. Data within a time window of ±2 h enter the statistical inter-comparison. The discrepancy between STDs retrieved from GPS data and their model equivalents is measured in terms of absolute and fractional differences:

$$\delta\mathrm{STD} = \mathrm{STD}_{ECMWF} - \mathrm{STD}_{GPS}$$
$$\delta\mathrm{STD}_{rel} = \frac{\delta\mathrm{STD}}{\mathrm{STD}_{ECMWF}} \tag{17}$$

According to Figure 4 the statistical inter-comparison from simulated SF and observed DF data indicates a good agree-

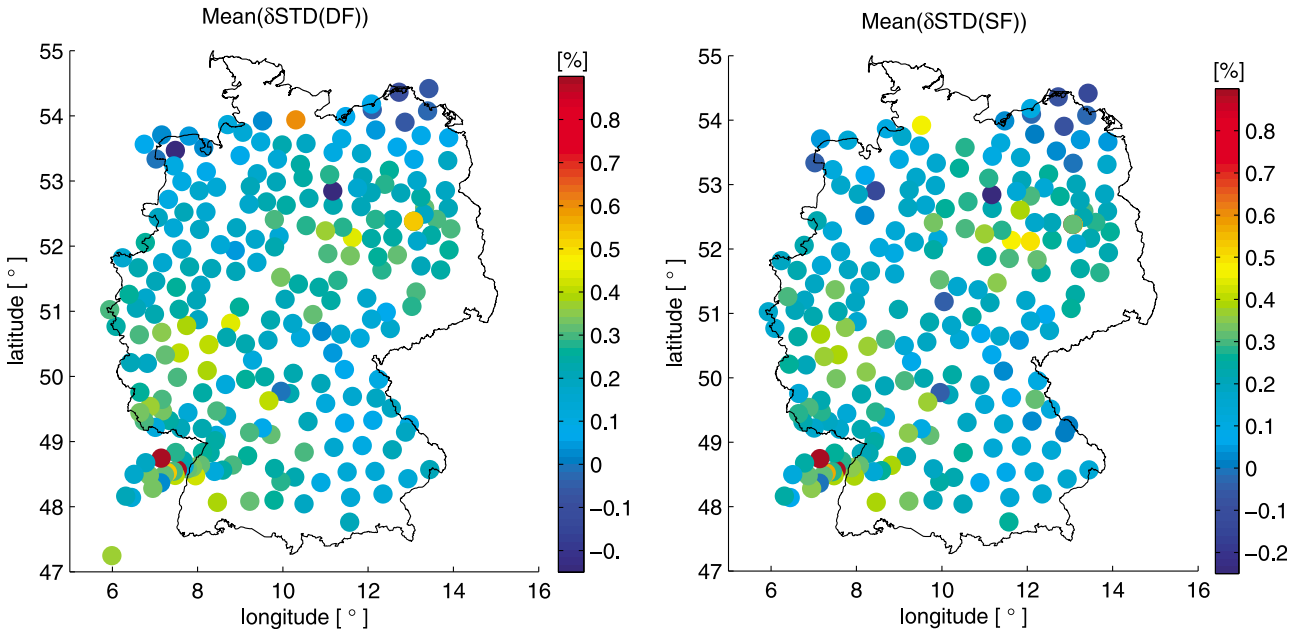

Figure 5. The fractional bias between GPS retrieved STDs (using SF and DF data) and STDs derived from the ECMWF analysis for each station. The left (right) panel corresponds to DF (SF) comparison.

ment over the entire elevation range. While the magnitude of absolute differences increases with decreasing elevation angles in case of SF and DF data, the fractional differences are almost constant. The bias of the fractional differences is ~0.2% in case of both SF and DF data (in the zenith this corresponds to 2.5 m · 0.2% ≈ 5 mm). The standard deviation of the fractional differences is ~0.55% for both SF and DF (in the zenith this corresponds to 2.5 m · 0.55% ≈ 14.7 mm). This finding is consistent with results obtained from comparable studies [*Pany et al.*, 2001; *Eresmaa et al.*, 2008]. The bias and the standard deviation for individual stations is shown in Figures 5 and 6. The biases are larger at stations located in north-east and south-west Germany while the standard deviations are enhanced at stations located in north-west Germany. A detailed analysis of this feature is beyond the scope of this study. No significant differences for simulated

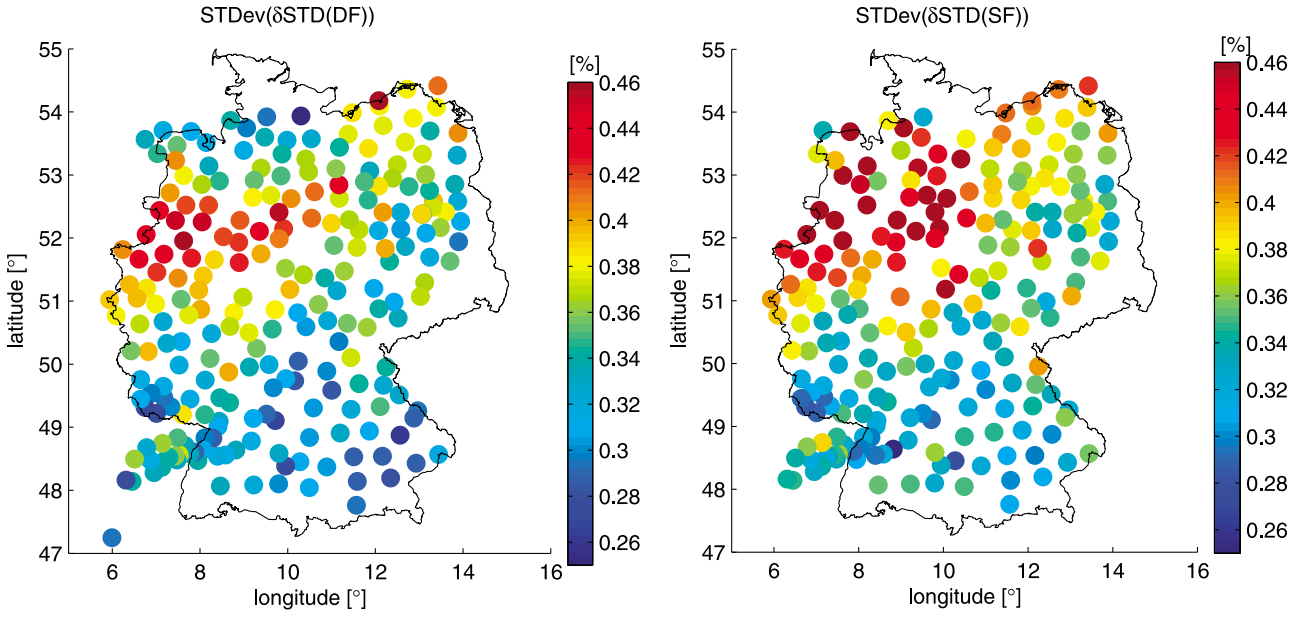

Figure 6. The fractional standard deviation between GPS retrieved STDs (using SF and DF data) and STDs derived from the ECMWF analysis for each station. The left (right) panel corresponds to DF (SF) comparison.

SF and observed DF data are found, i.e. STDs for both processing options show similar characteristics relative to their model equivalents for individual stations.

4.4. Slant Integrated Water Vapor From GPS and Water Vapor Radiometers

[29] Water Vapor Radiometers (WVR) can provide highly accurate observations of the integrated water vapor (SWV) along any given line of sight. These observations can be used to validate GPS STDs after separating the dry and wet contribution to the STD. The method described in section 2 was applied to both STD data sets to derive SWV data suitable for GPS-WVR comparisons. In zenith direction the SWV is almost identical to the IWV and varies usually between 5 and 50 kg m^{-2} at midlatitudes. In many validation studies [*Ware et al.*, 1997; *Braun et al.*, 2003] the IWV error was estimated to ~1.3 kg m^{-2} which is almost constant and independent from the total amount of water vapor in the atmosphere. Therefore, the relative error is rather large at dry days (>20%) and decreases considerably for very wet situations (<2%). As in case of the STD the SWV increases considerably with decreasing elevations.

[30] The radiometer observations available for this study were taken within the framework of the Convective and Orographically induced Precipitation Study (COPS) [*Wulfmeyer et al.*, 2008] which took place in 2007 in southwestern Germany/eastern France. The hemisphere-scanning Humidity and Temperature Profiler HATPRO [*Rose et al.*, 2005] of the University of Cologne was deployed on the roof of the US Atmospheric Radiation Measurement Program (ARM) Mobile Facility (AMF) in the Murg Valley, which is located in the northeastern part of the Black Forest, Germany (48.32°N, 8.23°E, 511 m above sea level). The site was located in the north-south oriented Murg Valley which is roughly 1 km wide. The WVR was placed 2 meter higher than the GPS station antenna and operated in full hemisphere scan mode between October and December 2007.

[31] The HATPRO is a 14-channel microwave radiometer observing atmospheric emission in two bands using seven channels between 22.235 and 31.4 GHz along the wing of the 22.235 GHz rotational water vapor line to derive the SWV via multilinear regression yielding accuracies better than 0.7 kg m^{-2}. The WVR observed at 36 azimuth angles every 10°, and at 8 elevation angles ranging from 14.4° to 90° leading to a total number of 288 observations per scan cycle distributed over the whole hemisphere. The elevations below 14.4° are not taken into account to avoid environmental influences. A whole hemisphere scan requires approximately 11 min.

[32] Since only a few WVR observations were performed exactly at the same time and in the same direction as the GPS observations, the SWVs were interpolated from the closest three WVR scans to the direction of the GPS observation. Using a linear interpolation the WVR-SWV values as well as tracking times were interpolated on the GPS observations.

[33] In the Black Forest region the atmosphere between October and December 2007 was relatively dry with the zenith IWVs varying from 10 to 20 kg m^{-2}. At the day of year 283 (October 10th, 2007) the IWV decreased from 17 kg m^{-2} in the morning down to 10 kg m^{-2} at midnight, and changed more intensely than the observed IWV at most other days. Assuming an absolute IWV error of 1 kg m^{-2} the relative IWV error at this day should be between 6% and 10%. For this day the SWVs derived from GPS STDs and the WVR were validated.

[34] In total 4349 (4168) SWVs from DF (SF) receivers were available and the WVR observations could be successfully interpolated for 3104 (3167) of these observations. As in the previous studies the absolute

$$\delta SWV = \mathrm{SWV}_{WVR} - \mathrm{SWV}_{GPS} \tag{18}$$

and fractional differences were investigated:

$$\delta SWV_{rel} = \frac{\delta SWV}{\mathrm{SWV}_{WVR}} \tag{19}$$

The absolute differences computed from all observations and all elevations show a very small bias of 0.2 kg m^{-2} (DF) and 0.5 kg m^{-2} (SF). The standard deviations of 1.7 kg m^{-2} = 6.8% (DF) and 1.6 kg m^{-2} = 6.1% (SF) provide no indication that the GPS SWV error should be much larger than the IWV error. The elevation-dependent differences (Figures 7 and 8) show an equally well agreement between GPS and WVR; for both cases and all elevations the bias is well below 1 kg m^{-2} or 5%. The standard deviation increases almost linearly from 1.3 kg m^{-2} near the zenith to about $\sigma = 2$ kg m^{-2} at $\varepsilon = 20°$. In case of relative differences σ decreases from >6% to ~5%. Even if the GPS-WVR differences were caused by the GPS SWV error alone this would be below the estimated IWV error. The elevation-dependent statistical quantities were computed in two ways, one is using a running window with 100 observations (gray and black lines), the other considers all values in each 10° elevation interval (blue and green stair lines). The increasing bias at elevations below ~30° is most presumably caused by the WVR data interpolation. As the radiometer is located down in the Murg Valley some mountains block the view in certain directions and only a limited number of observations can be interpolated to the GPS satellite direction.

[35] The result most important for this study is that there is no significant difference between the DF and SF data. The δSWV_{SF} data are even slightly smaller than the DF differences. This good result is very encouraging as several approximations had to be made on the GPS side to estimate the SWV: The SDD had to be estimated from the surface pressure at the GPS station to obtain the SWD and the surface temperature was required to estimate the conversion factor Π (equation (6)) which finally leads to the SWV. In case of the SF data the ionosphere correction is an additional potential uncertainty. Furthermore, the WVR did not point to the GPS satellites and the hemisphere scans had to be interpolated in order to get a sufficiently large WVR data set.

4.5. Validation Summary

[36] Three different validation studies were carried out, each one providing information of a different type. Analyzing the SF and DF GPS data sets provides mainly information on the ionosphere correction. ZTD and STD data could easily be compared and the quality of single stations could be observed as well as the network performance. This is also true for the validation with a numerical weather model. The model STDs could be estimated for a large number of stations but only at ECMWF analysis times, i.e., every 6 hours. In contrast to the first study the STD difference represents the observation

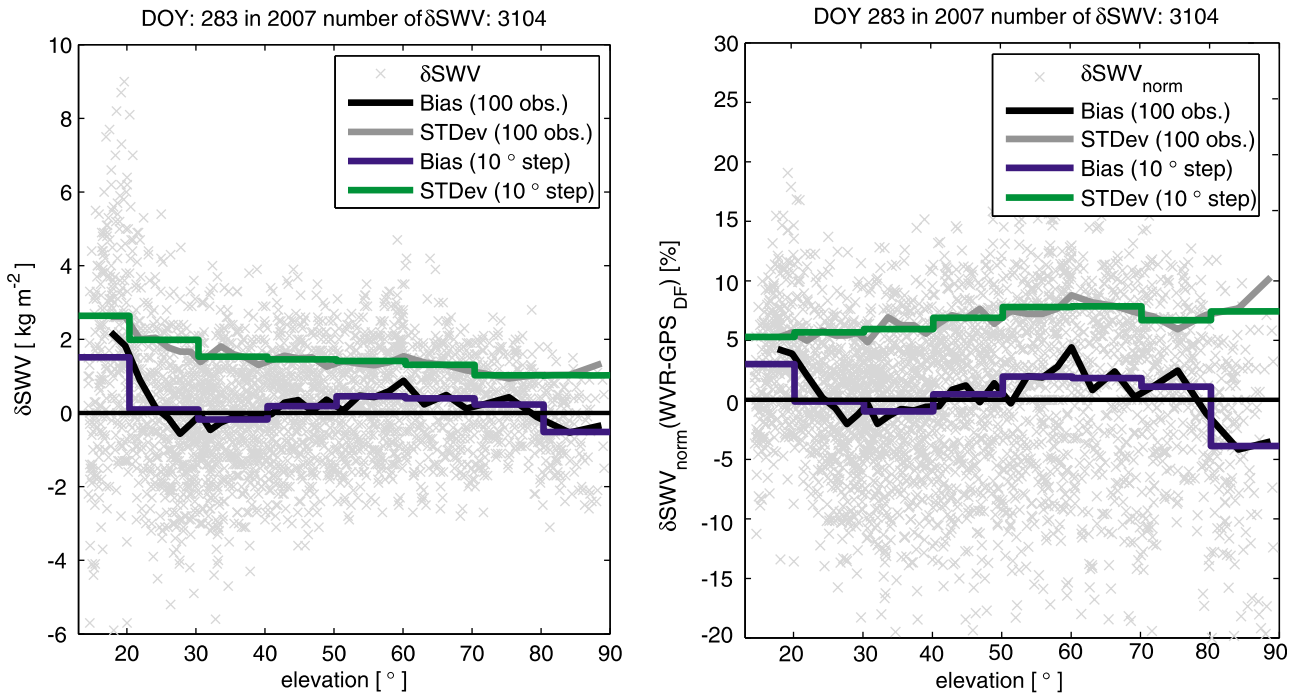

Figure 7. (left) The bias and the standard deviation between GPS DF retrieved SWVs and SWVs obtained from a WVR versus the elevation angle. (right) The fractional bias and standard deviation between GPS DF retrieved SWVs and SWVs obtained from a WVR versus the elevation angle.

errors of the GPS and model data and not only some differences in the processing strategy. In case of the radiometer validation the data of only one GPS station near the radiometer and only for one day could be analyzed. However, the radiometer was taking data continuously and provides observations with high quality. As the radiometer provides the SWV instead of STDs the GPS STDs had to be converted to the SWV and additional errors were introduced. The results

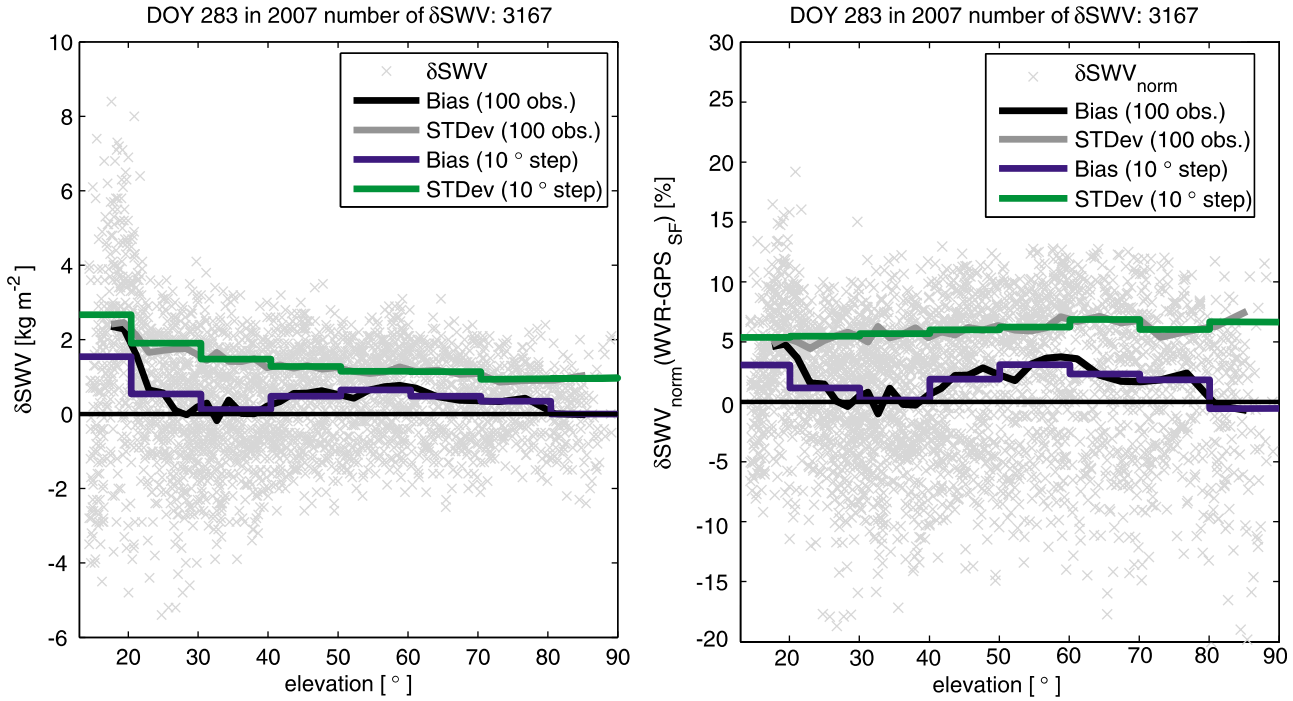

Figure 8. (left) The bias and the standard deviation between GPS SF retrieved SWVs and SWVs obtained from a WVR versus the elevation angle. (right) The fractional bias and standard deviation between GPS SF retrieved SWVs and SWVs obtained from a WVR versus the elevation angle.

Table 1. Summary of the Bias (μ), the Standard Deviation (σ), and the RMS for ZTD, STD, and SWV Comparisons (All in Zenith Direction)

Validation	Number of Stations	Number of Data	μ (mm)	σ (mm)	RMS (mm)
$ZTD_{(SF-DF)}$	258	$2.4 \cdot 10^5$	0.1	2.9	2.9
$STD_{(SF-DF)}$	258	$1.0 \cdot 10^7$	0.3	4.5	4.5
$STD_{(ECMWF-DF)}$	239	$7.9 \cdot 10^6$	5.2	13.0	14.0
$STD_{(ECMWF-SF)}$	232	$7.4 \cdot 10^6$	5.2	13.7	14.7
$SWD_{(WVR-DF)}$	1	$3.104 \cdot 10^3$	1.3	11.0	11.1
$SWD_{(WVR-SF)}$	1	$3.167 \cdot 10^3$	3.2	10.3	10.8

from the previous paragraphs are summarized in Table 1. To provide comparable quantities STD differences are obtained by multiplying fractional STD differences with a nominal ZTD value of 2.5 m. The SWD differences are obtained by multiplying SWV differences with the inverse conversion factor $\Pi^{-1} = 6.45$ (see equation (6)).

5. Conclusions

[37] A simulation study was carried out to estimate the potential of future large networks of SF receivers embedded in DF receiver networks. The focus was on GPS atmosphere sounding but the results are also relevant for other applications. One precondition for using SF receivers are reliable ionosphere corrections. The SEID method which utilizes the L_2 signals of nearby DF receivers was applied to a network of more than 270 DF receivers. For simulating SF stations each station in turn was regarded as a SF station by replacing the observed L_2 signal with the $\tilde{L}_2$ signal provided by SEID. It turned out that this method could be applied to almost all stations within the network. A good quality of the $\tilde{L}_2$ signals was found for most stations except some stations near the network boundaries and near some stations with known quality issues. These problems can easily be avoided when a real SF network is designed.

[38] The ZTD and STD observations obtained from the simulated SF data were compared to the corresponding DF data and to independent observations from a numerical weather model and a water vapor radiometer. The results of all three validation studies show that the ZTD and STD observations obtained from SF receivers are almost of the same quality as the DF observations. Comparing the DF data with the simulated SF data it could be shown that the $\tilde{L}_2$ signal estimated by SEID leads only to a small additional error. However, comparing both, the SF and the DF tropospheric products to other observations shows that the error of the SF data is smaller as could be expected from the first study. The quality of the SF data is fully sufficient for atmosphere sounding and the advantage of having more observations with improved spatial resolution is much higher than the drawback of the slightly increased noise. GPS observations are widely used because of their high sensitivity to atmospheric humidity. Due to the high spatiotemporal variability of water vapor neither interpolation techniques nor numerical weather models can estimate the water vapor field between the monitoring stations sufficiently well and more dense networks are required to provide observations of sufficient resolution. SF receivers could perform this task with minimal investments.

[39] In this simulation study some problems appearing with SF receivers could not be addressed. Increased receiver noise and multipath effects will reduce the quality of SF data and geodetic-grade SF receivers should be preferred. However, several SF studies showed that such problems could be resolved. The ionosphere corrections can be expected to become even better if the SF receivers were placed between the existing DF receivers thereby decreasing the distances between SF and DF stations.

[40] In a next step campaigns with an increasing number of real SF receivers will be started to show the applicability of the SEID method in different surroundings and to validate the quality of the SF products with more independent observations. Furthermore, the impact of SF data will be estimated by assimilating such observations to numerical weather models and by reconstructing spatially resolved humidity fields with the GPS tomography.

[41] **Acknowledgment.** This work was supported by Deutsche Forschungsgemeinschaft (DFG) within the priority Programme QPF 1167 and within the research project "APRO-GRAVAR" WI2634A-1.

References

Bar-Sever, Y. E., P. M. Kroger, and J. A. Borjesson (1998), Estimating horizontal gradients of tropospheric path delay with a single GPS receiver, *J. Geophys. Res.*, *103*(B3), 5019–5036.

Bender, M., G. Dick, M. Ge, Z. Deng, J. Wickert, H.-G. Kahle, A. Raabe, and G. Tetzlaff (2010), Development of a GNSS water vapor tomography system using algebraic reconstruction techniques, *Adv. Space Res.*, *47*(10), 1704–1720, doi:10.1016/j.asr.2010.05.034.

Bevis, M., S. Businger, S. Chiswell, T. A. Herring, R. A. Anthes, C. Rocken, and R. H. Ware (1994), GPS meteorology: Mapping zenith wet delays onto precipitable water, *J. Appl. Meteorol.*, *33*(3), 379–386, doi:10.1175/1520-0450.

Boehm, J., B. Werl, and H. Schuh (2006), Troposphere mapping functions for GPS and very long baseline interferometry from European Centre for Medium-Range Weather Forecasts operational analysis data, *J. Geophys. Res.*, *111*, B02406, doi:10.1029/2005JB003629.

Braun, J., C. Rocken, C. Meertens, and R. Ware (1999), Development of a water vapor tomography system using low cost L1 GPS receivers, paper presented at Ninth Annual ARM Science Team Meeting, Atmos. Radiat. Meas., San Antonio, Tex.

Braun, J., C. Rocken, and J. Liljegren (2003), Comparisons of line-of-sight water vapor observations using the global positioning system and a pointing microwave radiometer, *J. Atmos. Oceanic Technol.*, *20*(5), 606–612.

Brockmann, E., and M. Troller (2002), GPS Meteorology in the Swiss Alps: Interpolation Accuracy for different Alpine Areas and Near Real-time Results, paper presented at Exploitation of Ground-Based GPS for Meteorology, COST Action 716 Workshop, GeoForschungsZentrum Potsdam, Potsdam, Germany, 28–29 Jan.

Brunini, C., and F. Azpilicueta (2010), GPS slant total electron content accuracy using the single layer model under different geomagnetic regions and ionospheric conditions, *J. Geod.*, *84*, 293–304, doi:10.1007/s00190-010-0367-5.

Davis, J. L., G. Elgered, A. E. Niell, and C. E. Kuehn (1993), Ground-based measurement of gradients in the wet radio refractivity of air, *Radio Sci.*, *28*(6), 1003–1018.

Deng, Z., M. Bender, G. Dick, M. Ge, J. Wickert, M. Ramatschi, and X. Zou (2009), Retrieving tropospheric delays from GPS networks densified with single frequency receivers, *Geophys. Res. Lett.*, *36*, L19802, doi:10.1029/2009GL040018.

Dousa, J. (2001), Towards an operational near real-time precipitable water vapor estimation, *Phys. Chem. Earth A*, *26*(3), 189–194, doi:10.1016/S1464-1895(01)00045-X.

Eresmaa, R., S. Healy, H. Järvinen, and K. Salonen (2008), Implementation of a ray-tracing operator for ground-based GPS slant delay observation modeling, *J. Geophys. Res.*, *113*, D11114, doi:10.1029/2007JD009256.

Gendt, G., G. Dick, and W. Söhne (1999), GFZ analysis center of IGS—Annual report 1998, in *1998 Technical Reports*, edited by K. Gowey, R. Neilan, and A. Moore, pp. 79–87, Jet Propul. Lab., Pasadena, Calif.

Gendt, G., G. Dick, C. Reigber, M. Tomassini, Y. Liu, and M. Ramatschi (2004), Near real time GPS water vapor monitoring for numerical weather prediction in Germany, *J. Meteorol. Soc. Jpn.*, *82*(1B), 361–370.

Gutman, S. I., S. R. Sahm, S. G. Benjamin, B. E. Schwartz, K. L. Holub, J. Q. Stewart, and T. L. Smith (2004), Rapid retrieval and assimilation of ground based GPS precipitable water observations at the NOAA forecast systems laboratory: Impact on weather forecasts, *J. Meteorol. Soc. Jpn.*, *82*(1B), 351–360.

Haase, J., M. Ge, H. Vedel, and E. Calais (2003), Accuracy and variability of GPS tropospheric delay measurements of water vapor in the western mediterranean, *J. Appl. Meteorol.*, *42*(11), 1547–1568, doi:10.1175/1520-0450.

Hofmann-Wellenhof, B., H. Lichtenegger, and J. Collins (2001), *GPS: Theory and Practice*, Springer, New York.

Jakowski, N., C. Mayer, C. Borries, and T. Pannowitsch (2009), Large and mid-scale ionospheric perturbation characteristics deduced from GNSS measurements, *IET Conf. Publ.*, *2009*(CP549), 210–214, doi:10.1049/cp.2009.0065.

Janssen, V., and C. Rizos (2005), Mixed-mode GPS deformation monitoring—A cost-effective and accurate alternative?, in *A Window on the Future of Geodesy, International Association of Geodesy Symposia*, vol. 128, edited by F. Sansó and F. Sansó, pp. 533–537, Springer, Heidelberg, Germany.

Järvinen, H., R. Eresmaa, H. Vedel, K. Salonen, S. Niemelä, and J. de Vries (2007), A variational data assimilation system for ground-based GPS slant delays, *Q. J. R. Meteorol. Soc.*, *133*, 969–980, doi:10.1002/qj.79.

Pany, T., P. Pesec, and G. Stangl (2001), Atmospheric GPS slant path delays and ray tracing through numerical weather models, a comparison, *Phys. Chem. Earth A*, *26*(3), 183–188, doi:10.1016/S1464-1895(01)00044-8.

Poli, P., P. Moll, F. Rabier, G. Desroziers, B. Chapnik, L. Berre, S. B. Healy, E. Andersson, and F. E. Guelai (2007), Forecast impact studies of zenith total delay data from European near real-time GPS stations in Météo France 4DVAR, *J. Geophys. Res.*, *112*, D06114, doi:10.1029/2006JD007430.

Rocken, C., M. Johnson, and J. Braun (2000), Improving GPS surveying with modeled ionospheric corrections, *Geophys. Res. Lett.*, *27*(23), 3821–3824.

Rose, T., S. Crewell, U. Löhnert, and C. Simmer (2005), A network suitable microwave radiometer for operational monitoring of the cloudy atmosphere, *Atmos. Res.*, *75*, 183–200.

Saastamoinen, J. (1973), Contributions to the theory of atmospheric refraction Part II. Refraction corrections in satellite geodesy, *Bull. Geod.*, *107*, 13–34.

Schaer, S. (1999), Mapping and predicting the Earth's ionosphere using the GPS, Ph.D. thesis, Univ. Bern, Bern, Switzerland.

Schmid, R., M. Rothacher, D. Thaller, and P. Steigenberger (2005), Absolute phase center corrections of satellite and receiver antennas, *GPS Solutions*, *9*, 283–293, doi:10.1007/s10291-005-0134-x.

Shoji, Y. (2009), A study of near real-time water vapor analysis using a nationwide dense GPS network of Japan, *J. Meteorol. Soc. Jpn.*, *87*, 1–18, doi:10.2151/jmsj.87.1.

Sokolovskiy, S., C. Rocken, and A. Lowry (2001), Use of GPS for estimation of bending angles of radio waves at low elevations, *Radio Sci.*, *36*(3), 473–482.

Solheim, F., J. Vivekandanan, R. Ware, and C. Rocken (1999), Propagation delays induced in GPS signals by dry air, water vapor, hydrometeors and other particulate, *J. Geophys. Res.*, *104*(D8), 9663–9670.

Tralli, D. M., and S. M. Lichten (1990), Stochastic estimation of tropospheric path delays in global positioning system geodetic measurements, *J. Geod.*, *64*(2), 127–159, doi:10.1007/BF02520642.

Wanninger, L. (1995), Enhancing differential GPS using regional ionospheric error models, *Bull. Geod.*, *69*, 283–291.

Ware, R., C. Alber, C. Rocken, and F. Solheim (1997), Sensing integrated water vapor along GPS ray paths, *Geophys. Res. Lett.*, *24*(4), 417–420, doi:10.1029/97GL00080.

Wulfmeyer, V., et al. (2008), The convective and orographically-induced precipitation study: A research and development project of the World Weather Research program for improving quantitative precipitation forecasting in low-mountain regions, *Bull. Am. Meteorol. Soc.*, *89*(10), 1477–1486, doi:10.1175/2008BAMS2367.1.

Zumberge, J. F., M. B. Heflin, D. C. Jefferson, M. M. Watkins, and F. H. Webb (1997), Precise point positioning for the efficient and robust analysis of GPS data from large networks, *J. Geophys. Res.*, *102*(B3), 5005–5018, doi:10.1029/96JB03860.

Zus, F. (2010), Application of Global Positioning System slant path delay data for mesoscale model verification and four-dimensional variational assimilation, Ph.D. thesis, Hohenheim Univ., Stuttgart, Germany.

M. Bender, Z. Deng, G. Dick, M. Ge, M. Ramatschi, J. Wickert, and F. Zus, GPS/Galileo Earth Observation, Helmholtz-Zentrum Potsdam, Deutsches GeoForschungsZentrum, Telegrafenberg, D-14473 Potsdam, Germany. (bender@gfz-potsdam.de; deng@gfz-potsdam.de; dick@gfz-potsdam.de; maor@gfz-potsdam.de; maram@gfz-potsdam.de; wickert@gfz-potsdam.de; zusflo@gfz-potsdam.de)

U. Löhnert, Institute for Geophysics and Meteorology, University of Cologne, D-50674 Cologne, Germany. (loehnert@meteo.uni-koeln.de)

S. Schön, Institut für Erdmessung, Leibniz Universität Hannover, D-30167 Hannover, Germany. (schoen@ife.uni-hannover.de)